

A FORMULATION FOR FULLY RESOLVED SIMULATION (FRS) OF PARTICLE-TURBULENCE INTERACTIONS IN TWO-PHASE FLOWS

SOURABH V. APTE AND NEELESH A. PATANKAR

Abstract. A numerical formulation for fully resolved simulations of freely moving rigid particles in turbulent flows is presented. This work builds upon the fictitious-domain based approach for fast computation of fluid-rigid particle motion by Sharma & Patankar ([1] Ref. J. Compt. Phy., (205), 2005). The approach avoids explicit calculation of distributed Lagrange multipliers to impose rigid body motion and reduces the computational overhead due to the particle-phase. Implementation of the numerical algorithm in co-located, finite-volume-based, energy conserving fractional-step schemes on structured, Cartesian grids is presented. The numerical approach is first validated for flow over a fixed sphere at various Reynolds numbers and flow generated by a freely falling sphere under gravity. Grid and time-step convergence studies are performed to evaluate the accuracy of the approach. Finally, simulation of 125 cubical particles in a decaying isotropic turbulent flow is performed to study the feasibility of simulations of turbulent flows in the presence of freely moving, arbitrary-shaped rigid particles.

Key Words. DNS, particle-turbulence interactions, point-particle, fully resolved particles.

1. Introduction

Many problems in nature and engineering involve two-phase flows where solid particles of arbitrary shape and sizes are dispersed in an ambient fluid (gas or liquid) undergoing time dependent and often turbulent motion. Examples include sediment transport in rivers, fluidized beds, coal-based oxy-fuel combustion chambers, biomass gasifiers, among others. These applications involve common physical phenomena, at disparate length and time scales, of mass, momentum, and energy transport across the interface between the dispersed particles and a continuum fluid.

Numerical simulations of these flows commonly employ Lagrangian description for the dispersed phase and Eulerian formulation for the carrier phase. Depending on the volumetric loading of the dispersed phase two regimes are identified: dilute ($d_p \ll \ell$) and dense ($d_p \approx \ell$), where d_p is the characteristic length scale of the particle (e.g. diameter), and ℓ the inter-particle distance. Furthermore, the grid resolution (Δ) used for solution of the carrier phase could be such that the particles are ‘subgrid’ ($d_p \ll \Delta$), ‘partially resolved’ ($d_p \sim \Delta$), or ‘fully resolved’ ($\Delta < d_p$). In addition, these regimes may occur in the same problem and are dependent on the particle size as well as the grid resolution. Clearly, multiscale numerical approaches are necessary to simulate various regimes of the flow.

The standard approach to simulate turbulent particle-laden flows uses direct numerical simulation (DNS) [2, 3, 4], large-eddy simulation (LES) [5, 6, 7, 8] or Reynolds-Averaged Navier Stokes (RANS) approach [9] for the carrier phase whereas the motion of the dispersed phase is modeled. In all these approaches, the particles are assumed ‘point-sources’ compared to the grid resolutions used (so $d_p < \eta$, the Kolmogorov length scale, for DNS whereas $d_p < \Delta$, the grid size, in LES or RANS). The fluid volume displaced by the particles are presumed negligible. Recently, an improved approach, based on mixture theory and considering the volumetric displacements of the fluid by the particles was developed for DNS/LES of particle-laden flows [10]. However, both of these approaches model the interactions between the fluid and the particles, use drag and lift correlations to approximate the drag and lift forces on the particles. The accuracy of these approaches in capturing the complex particle-fluid interactions in turbulent flows depends on the validity of simplified drag and lift laws.

Fully resolved simulation (FRS) of these flows require grid resolutions finer than the characteristic size of particles. In this approach, all scales associated with the particle motion are resolved and the drag/lift forces on the particles are *directly* evaluated rather than modeled. Considerable work has been done on fully resolved simulations of particles in laminar flows. Arbitrary Lagrangian-Eulerian (ALE) method [11], distributed Lagrange multiplier/fictitious domain (DLM) based methods [12, 13, 14], Lattice Boltzmann (LBM) [15], and Immersed Boundary (IBM) based methods [16, 17, 18] have been proposed and used. These methods have been applied to simulate a modest number of particles (around 1000s) at low Reynolds numbers. In spite of several different numerical schemes, full three-dimensional direct simulations of two-phase turbulent flows in realistic configurations are rare. There are only few three-dimensional turbulent flow studies in canonical configurations on fully resolved rigid particles [19, 20]. There appears to be no reported study of fully resolved moving particles in complex geometries. In the present work, a fictitious domain based approach for motion of arbitrary rigid particles is implemented in a structured finite-volume solver capable of simulating turbulent flows. The approach is based on an efficient numerical algorithm proposed by Patankar [21] to constrain the flow field inside the particle to a rigid body motion. This facilitates simulation of large-number of particles by reducing the overhead associated with the computation of particle motion.

The paper is arranged as follows. A mathematical formulation of the basic scheme is described briefly. Numerical implementation of the scheme in a co-located grid, finite volume framework is provided next. The numerical scheme is validated for flow over a fixed sphere at different Reynolds numbers and a freely falling sphere under gravity. Simulation of 125 cubic particles in an isotropic turbulent flow is then performed to show the feasibility of the approach to capture multiscale interactions between the particles and unsteady turbulent flows.

2. Mathematical Formulation

Let Γ be the computational domain which includes both the fluid (Γ_F) and the particle ($\Gamma_P(t)$) domains. Let the fluid boundary not shared with the particle be denoted by \mathcal{B} and have a Dirichlet condition. For the present work, focus is placed on flows in closed domains and thus number of particles inside the computational domain remains fixed. Further evaluation of generalized boundary conditions is necessary for inflow-outflow systems where number of particles inside the domain may vary with time. For simplicity, let there be a single particle in the domain

and the body force be assumed constant so that there is no net torque acting on the particle. The basis of fictitious-domain based approach [12] is to extend the Navier-Stokes equations for fluid motion over the entire domain Γ inclusive of particle regions. The natural choice is to assume that the particle region is filled with a Newtonian *fluid* of density equal to the particle density (ρ_P) and some fluid viscosity (μ_F). Both the fluid and the particle regions will be assumed as incompressible and thus incompressibility constraint applies over the entire region. In addition, as the particles are assumed as rigid, the motion of the material inside the particle is constrained to be a rigid body motion. Several ways of obtaining the rigidity constraint have been proposed [12, 13, 21, 14]. We follow the formulation developed by Patankar [21] which is briefly described for completeness.

The momentum equation for fluid motion applicable in the entire domain Γ is given by:

$$(1) \quad \rho \left(\frac{\partial \mathbf{u}}{\partial t} + (\mathbf{u} \cdot \nabla) \mathbf{u} \right) = -\nabla p + \nabla \cdot \left(\mu_F \left(\nabla \mathbf{u} + (\nabla \mathbf{u})^T \right) \right) + \rho \mathbf{g} + \mathbf{f},$$

where ρ is the density field, \mathbf{u} the velocity vector, p the pressure, μ_F the fluid viscosity, \mathbf{g} the gravitational acceleration, and \mathbf{f} is an additional body force that enforces rigid body motion inside the particle region Γ_P . For direct numerical simulations of incompressible fluid as considered in this work, μ_F is the dynamic viscosity of the fluid. It is assumed to be constant and the viscous term can be simplified to $\mu_F \nabla^2 \mathbf{u}$ using the incompressibility constraint. The viscosity μ_F is defined at the *cv* centers and then evaluated at the faces using simple arithmetic averages. In the case where the grid resolution is such that all scales of turbulence are not captured, turbulence closure may be obtained using large-eddy simulations (LES) or Reynolds Averaged Navier Stokes (RANS) models. The viscosity μ_F will then be replaced by the eddy viscosity as provided by closure models used in either approaches. However, it should be noted that the turbulence closure models are valid in the bulk flow (far from the boundary). Near the moving boundary, wall modeling techniques may become necessary.

The density ρ is given as:

$$(2) \quad \rho = \rho_F(1 - \Theta_P) + \rho_P \Theta_P; \quad \Theta_P = \begin{cases} 0 & \text{in } \Gamma_F \\ 1 & \text{in } \Gamma_P \end{cases}$$

where ρ_F and ρ_P are the fluid and particle densities, respectively, Θ_p is the indicator function that assumes a value of unity inside the particle region and zero outside. In general numerical implementations, the indicator function is smeared over a small region (proportional to the grid spacing) around the boundary giving a smooth variation. As the particle moves, so does the indicator function and thus $D\Theta_p/Dt = 0$ on the particle boundary, where $D/Dt()$ represents a material derivative. The continuity equation in Γ for this variable density Newtonian fluid is given as:

$$(3) \quad \frac{\partial \rho}{\partial t} + \nabla \cdot (\rho \mathbf{u}) = 0.$$

Using the definition of ρ , expanding the above equation and noting than $D\Theta_p/Dt = 0$ on the particle boundaries gives the incompressibility constraint over the entire domain Γ :

$$(4) \quad \nabla \cdot \mathbf{u} = 0,$$

In order to enforce that the material inside the particle region moves in a rigid fashion, a rigidity constraint is required so that it will lead to a non-zero forcing function \mathbf{f} in the particle region. Different ways have been proposed to obtain \mathbf{f} .

Inside the particle region, the rigid body motion implies vanishing deformation rate tensor:

$$(5) \quad \left. \begin{aligned} \frac{1}{2} (\nabla \mathbf{u} + (\nabla \mathbf{u})^T) &= \mathbf{D}[\mathbf{u}] = 0, \\ \mathbf{u} &= \mathbf{u}^{RBM} = \mathbf{U} + \Omega \times \mathbf{r} \end{aligned} \right\} \text{ in } \Gamma_P,$$

where \mathbf{U} and Ω are the particle translation and angular velocities and \mathbf{r} is the position vector of a point inside the particle region from the particle centroid. The vanishing deformation rate tensor for rigidity constraint automatically ensures the incompressibility constraint inside the particle region. The incompressibility constraint gives rise to the scalar field (the pressure, p) in a fluid. Similarly, the tensor constraint $\mathbf{D}[\mathbf{u}] = 0$ for rigid motion gives rise to a tensor field inside the particle region [13]. Distributed Lagrange multipliers (DLM)-based approaches have been proposed to solve for the rigid body motion and impose the rigidity constraint which requires an iterative solution strategy. Patankar [21] proposed an approach that provides the rigidity constraint explicitly, thus reducing the computational cost significantly. Noting that the tensorial rigidity constraint can be reformulated to give:

$$(6) \quad \nabla \cdot (\mathbf{D}[\mathbf{u}]) = 0 \text{ in } \Gamma_P;$$

$$(7) \quad \mathbf{D}[\mathbf{u}] \cdot \mathbf{n} = 0 \text{ on particle boundary.}$$

a two-stage fractional-step algorithm can be devised to solve the coupled fluid-particle problem [21]. Knowing the solution at time level t^n the goal is to find \mathbf{u} at time t^{n+1} .

- (1) In this first step, the rigidity constraint force \mathbf{f} in equation 1 is set to zero and the equation together with the incompressibility constraint (equation 4) is solved by standard fractional-step schemes over the entire domain. Accordingly, a pressure Poisson equation is derived and used to project the velocity field onto an incompressible solution. The obtained velocity field is denoted as \mathbf{u}^{n+1} inside the fluid domain and $\hat{\mathbf{u}}$ inside the particle region.
- (2) The velocity field in the particle domain is obtained in a second step by projecting the flow field onto a rigid body motion. Inside the particle region:

$$(8) \quad \rho_P \left(\frac{\mathbf{u}^{n+1} - \hat{\mathbf{u}}}{\Delta t} \right) = \mathbf{f}.$$

To solve for \mathbf{u}^{n+1} inside the particle region we require \mathbf{f} . Obtaining the deformation rate tensor from \mathbf{u}^{n+1} given by the above equation and using the equations (6, 7) we obtain:

$$(9) \quad \nabla \cdot (\mathbf{D}[\mathbf{u}^{n+1}]) = \nabla \cdot \left(\mathbf{D} \left[\hat{\mathbf{u}} + \frac{\mathbf{f}\Delta t}{\rho} \right] \right) = 0;$$

$$(10) \quad \mathbf{D}[\mathbf{u}^{n+1}] \cdot \mathbf{n} = \mathbf{D} \left[\hat{\mathbf{u}} + \frac{\mathbf{f}\Delta t}{\rho} \right] \cdot \mathbf{n} = 0.$$

The velocity field in the particle domain involves only translation and angular velocities. Thus $\hat{\mathbf{u}}$ is split into a rigid body motion ($\mathbf{u}^{RBM} = \mathbf{U} + \Omega \times \mathbf{r}$) and residual non-rigid motion (\mathbf{u}'). The translational and rotational components of the rigid body motion are obtained by conserving the linear and angular momenta and

are given as:

$$(11) \quad M_P \mathbf{U} = \int_{\Gamma_P} \rho \hat{\mathbf{u}} d\mathbf{x};$$

$$(12) \quad \mathbf{I}_P \Omega = \int_{\Gamma_P} \mathbf{r} \times \rho \hat{\mathbf{u}} d\mathbf{x},$$

where M_P is the mass of the particle and $\mathbf{I}_P = \int_{\Gamma_P} \rho[(\mathbf{r} \cdot \mathbf{r})\mathbf{I} - \mathbf{r} \otimes \mathbf{r}]d\mathbf{x}$ is the moment of inertia tensor. Knowing \mathbf{U} and Ω for each particle, the rigid body motion inside the particle region \mathbf{u}^{RBM} can be calculated. The rigidity constraint force is then simply obtained as $\mathbf{f} = \rho(\mathbf{u}^{RBM} - \hat{\mathbf{u}})/\Delta t$. This sets $\mathbf{u}^{n+1} = \mathbf{u}^{RBM}$ in the particle domain. Note that the rigidity constraint is non-zero only inside the particle domain and zero everywhere else. In practice, the fluid flow near the boundary of the particle (over a length scale on the order of the grid size) is altered by the above procedure owing to the smearing of the particle boundary.

The key advantage of the above formulation is that the projection step only involves integrations in the particle domain with no iterations. A similar approach was recently proposed in a finite-element framework by Veeramani *et al.* [14].

3. Numerical Implementation

The above formulation was implemented and tested in a finite-volume method on staggered grids by Sharma & Patankar [1]. However, their work was limited to laminar flows and few number of particles. In this paper, we present the implementation of the above formulation in an energy-conserving, co-located grid finite-volume method. The original single-phase fluid flow solver is based on that developed by Mahesh *et al.* [23] on arbitrary shaped, unstructured grids. The main advantage of this single phase flow algorithm is that it is directly applicable to turbulent flows where numerical dissipation is undesirable. We use their approach on a simple, uniform Cartesian grids, however, the scheme can be readily implemented into an unstructured grid solver for complex configurations.

Figure 1a shows the schematic of variable storage in space. All variables are stored at the control volume (*cv*) center with the exception of the face-normal velocity u_N , located at the face centers. The face-normal velocity is used to enforce continuity equation. Capital letters are used to denote particle fields. We follow the collocated spatial arrangement for velocity and pressure field as has been used by [24, 25, 23, 26]. The main reason to use this arrangement as opposed to spatial-staggering is the flexibility of extending the scheme to unstructured grids and/or adaptive mesh refinement.

Figure 1b shows the arrangement of material volumes for cubic or spherical particles. Each material volume is cubic has a characteristic length (Δ_M) which can be compared with the background grid resolution Δ . Usually, $\Delta/\Delta_M \geq 2$ is used for better approximations of interpolated quantities between the background grid and the material volumes. In this work, conservative interpolation kernels similar to those used in Immersed Boundary Methods (IBM) are used for interpolations [22]. For example, computation of an Eulerian volume fraction field, $\Theta_p(\mathbf{x})$, from the material points at \mathbf{x}_k is performed as:

$$(13) \quad \Theta_p(\mathbf{x}) = \sum_{k=1}^{N_m} V_k \delta_{\Delta}^3(\mathbf{x} - \mathbf{x}_k),$$

where $V_k = \Delta_M^3$ is the volume associated with each material point and δ_{Δ}^3 is a delta function used for interpolation. In this work, a three-point delta-function

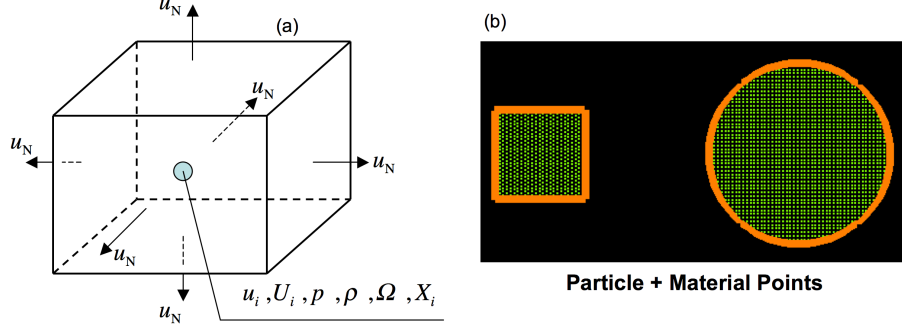


FIGURE 1. (a) Schematic of the variable storage for a co-located grid finite-volume scheme. The velocity field (u_N) represents the *face-normal* velocity and is used to enforce continuity constraint. The velocities u_i represent the Cartesian components and are co-located with the volume fraction (Θ), density (ρ), pressure (p), particle position (X_i), and the rigidity constraint force $F_{i,R}$ at the control volume (cv) centroid. In this co-located formulation, the face-normal velocity u_N is used to enforce the continuity constraint. (b) Schematic of material volume representation of particles. Each particle domain consists of cubic material volumes which retain their position with respect to the centroid of the particle. Interpolations between material volumes and background grids are used to calculate Eulerian fields such as volume fractions.

with compact support is used. In three-dimensions, the kernel is given as:

$$(14) \quad \delta_{\Delta}^3(\mathbf{x} - \mathbf{x}_k) = \frac{1}{\Delta^3} \xi\left(\frac{x - x_k}{\Delta}\right) \xi\left(\frac{y - y_k}{\Delta}\right) \xi\left(\frac{z - z_k}{\Delta}\right),$$

where the function ξ is given as:

$$(15) \quad \xi(r) = \begin{cases} \frac{1}{6}(5 - 3|r| - \sqrt{-3(1 - |r|)^2 + 1}), & 0.5 \leq |r| \leq 1.5, r = \frac{(x - x_0)}{\Delta} \\ \frac{1}{3}(1 + \sqrt{-3r^2 + 1}), & |r| \leq 0.5 \\ 0, & \text{otherwise} \end{cases}$$

The same interpolation kernel is used to interpolate an Eulerian quantity defined at the grid centroids to the material volume centroids. The interpolation kernel is second order accurate for smoothly varying fields [22].

Assuming that the solution at time level t^n is known, the following steps are performed to advance the fluid and particle velocity fields and the particle positions to time level t^{n+1} . Integrating the governing equations over the control volume and applying Gauss' divergence theorem to convert volume integrals to surface integrals wherever possible, the discrete governing equations are derived. Accordingly, the continuity equation is

$$(16) \quad \frac{\rho_{cv}^{n+1} - \rho_{cv}^n}{\Delta t} + \frac{1}{V_{cv}} \sum_{\text{faces of } cv} \rho_{face}^{n+1} u_N^{n+1} A_{face} = 0$$

where the subscript “*face*” corresponds to the face-center, A_{face} is the face area, V_{cv} the volume of the control volume, and u_N is the face-normal velocity. The density field (at any discrete time) is a linear function of the volume fraction and is given by equation (2). The particle volume fraction is a function of the position

of the particle and is obtained by interpolation procedure described above. Note that for a single phase, incompressible fluid, the above continuity equation becomes the incompressibility constraint $\sum_{\text{faces of cv}} u_N^{n+1} A_{\text{face}} = 0$. For the particle-laden computational domain, it also enforces the same constraint inside the fluid and particle regions. Changes in density are non-zero only near the interface, due to smearing of the particle boundary using the above interpolation kernels.

The discrete momentum equation for the i^{th} component of velocity is

$$(17) \quad \frac{\rho_{cv}^{n+1} u_{i,cv}^{n+1} - \rho_{cv}^n u_{i,cv}^n}{\Delta t} + \frac{1}{V_{cv}} \sum_{\text{faces of cv}} \rho_{\text{face}}^{n+1/2} u_{i,\text{face}}^{n+1/2} u_N^{n+1/2} A_{\text{face}} = -\frac{\partial}{\partial x_i} p_{cv}^{n+1} + \frac{1}{V_{cv}} \sum_{\text{faces of cv}} (\tau_{ij})_{\text{face}}^{n+1/2} N_{j,\text{face}} A_{\text{face}} + f_{i,cv}^{n+1},$$

where $(\tau_{ij})_{\text{face}}$ is the viscous stress at the faces of control volume, and $N_{j,\text{face}}$ represents the components of the outward face-normal. The velocity field $(u_{i,\text{face}})$ and the density (ρ_{face}) at the faces are obtained using arithmetic averages of the corresponding fields at two control volumes associated with the face. The interaction force f_i is used to impose the rigidity constraint within the particle domain. The above equations are solved using the fractional-step algorithm:

- (1) Advance the particle positions An explicit update of the particle position is performed.

$$X_{i,P}^{n+1} = X_{i,P}^n + \Delta t U_{i,P}^{n+1/2}$$

An Adams-Bashforth predictor is used to obtain the particle velocity at the midpoint in time, $U_{i,p}^{n+1/2} = \frac{3}{2} U_{i,p}^n - \frac{1}{2} U_{i,p}^{n-1}$. For non-spherical particles, it is also necessary to advance the angular orientation of the particle about its centroid. Knowing the angular velocity at the material points $\Omega_{i,M}^{n+1/2}$, it is straight forward to obtain their new orientation with respect to the particle centroid.

- (2) Evaluate Θ_P^{n+1} , ρ_{cv}^{n+1} using the equation 2
- (3) Solve the momentum equations for the cell-centered velocities to obtain a predictor $(\hat{u}_{i,cv}^{n+1})$ without the rigidity constraint $(f_{i,cv}^{n+1})$.

$$\frac{\rho_{cv}^{n+1} \hat{u}_{i,cv}^{n+1} - \rho_{cv}^n u_{i,cv}^n}{\Delta t} + \frac{1}{V_{cv}} \sum_{\text{faces of cv}} \rho_{\text{face}}^{n+1/2} u_{i,\text{face}}^{n+1/2} u_N^{n+1/2} A_{\text{face}} = -\frac{\partial}{\partial x_i} p_{cv}^n + \frac{1}{V_{cv}} \sum_{\text{faces of cv}} (\tau_{ij})_{\text{face}}^{n+1/2} N_{j,\text{face}} A_{\text{face}}$$

Arithmetic averages are used in time and space to evaluate the densities at $t^{n+1/2}$ and faces of a control volume. A Gauss-Seidel iterative solution scheme is used to solve the above non-linear partial differential equations. Second-order Adams-Bashforth predictor is used for the face-normal velocities $u_N^{n+1/2}$.

- (4) Remove the old pressure gradient

$$\frac{\rho_{cv}^{n+1} u_{i,cv}^* - \rho_{cv}^{n+1} \hat{u}_{i,cv}}{\Delta t} = +\frac{\partial}{\partial x_i} (p_{cv}^n)$$

- (5) Solve the Poisson equation for pressure to impose the continuity constraint

$$\sum_{\text{faces of cv}} \frac{\delta}{\delta N} (p_{cv}^{n+1}) A_{\text{face}} = \frac{1}{\Delta t} \sum_{\text{face of cv}} \rho_{\text{face}}^{n+1} u_N^* A_{\text{face}} + V_{cv} \frac{\delta}{\Delta t} (\rho_{cv}^{n+1})$$

where $u_N^* = 0.5(u_{i,nbr1}^* + u_{i,nbr2}^*)N_i$, is the face-normal velocity at the faces of control volumes obtained as an arithmetic average of the velocities at the neighboring control volumes ($nbr1$ and $nbr2$). The pressure Poisson equation is solved using *HYPRE*, the Algebraic Multi Grid (AMG) libraries, developed at Lawrence Livermore National Laboratory [27].

- (6) Correct the velocity field by projecting out the continuity constraint. The corrected cv -center based velocity field is denoted as $u_{i,cv}^{*n+1}$ as it may not satisfy the rigidity constraint in the particle domain. This is corrected further in following steps. In a co-located grid formulation, the role of the face-normal velocity u_N^{n+1} is to enforce continuity equation. This is obtained by projecting out the face-normal pressure gradient:

$$\begin{aligned} \rho_{cv}^{n+1} \frac{(u_{i,cv}^{*n+1} - u_{i,cv}^*)}{\Delta t} &= -\frac{\partial}{\partial x_i} p_{cv}^{n+1} \\ \rho_{face}^{n+1} \frac{(u_N^{*n+1} - u_N^*)}{\Delta t} &= -\frac{\partial}{\partial N} p_{cv}^{n+1} \end{aligned}$$

Note that it is important to properly re-construct the pressure gradient at the cv -centers $\partial p_{cv}^{n+1} / \partial x_i$. Mahesh *et al.* [23, 26] developed a face-area weighted least-squares based reconstruction that was shown to give stable and accurate results for high Reynolds number turbulent flows on arbitrary shaped, unstructured grids. We use the same algorithm here to reconstruct the pressure gradient at the cv -centers by minimizing the following expression in a least-squares sense:

$$\epsilon_{cv} = \sum_{\text{faces of cv}} \left(\frac{\partial}{\partial x_i} p_{cv}^{n+1} N_{i,face} - \frac{\partial}{\partial N} p_{cv}^{n+1} \right)^2 A_{face},$$

with

$$\frac{\partial}{\partial N} p_{cv}^{n+1} = \frac{p_{nbr}^{n+1} - p_{cv}^{n+1}}{\|s_{cv,nbr}\|}$$

where $\|s_{cv,nbr}\|$ is the length of the vector connecting between the nbr and cv control volumes associated with a $face$.

- (7) Evaluate the rigid body motion for each particle by calculating the translational and rotational velocity components:

$$\begin{aligned} M_P \mathbf{U}_P^{n+1} &= \sum_{k=1}^M \rho_P \mathbf{U}_M^{*n+1} V_k; \\ \mathbf{I}_P \Omega_P^{n+1} &= \sum_{k=1}^M (\mathbf{r} \times \rho_P \mathbf{U}_M^{*n+1}) V_k, \end{aligned}$$

where M_P and \mathbf{I}_P are the mass and moment of inertia for the particle P , the summation is over all material points M within the particle P , $V_k (= \Delta_M^3)$ is the volume of each material point, ρ_P is the density of the particle, \mathbf{U}_M^{*n+1} is the velocity field at the material point M obtained via interpolation from the velocity field (\mathbf{u}_{cv}^{*n+1} at the neighboring control volumes, \mathbf{r} is the position vector of each material point from the centroid of the particle P . The interpolations are performed using the three-point delta function given by equation 14.

- (8) The rigid body motion at each material point is given as $\mathbf{U}_M^{n+1,RBM} = \mathbf{U}_P^{n+1} + \Omega_P^{n+1} \times \mathbf{r}$. This can be interpolated to the computational grid using

the delta functions to obtain the rigid body motion $\mathbf{u}^{n+1,RBM}$ and the rigidity constraint force $f_{i,cv}^{n+1}$ at the cv centers:

$$\begin{aligned} f_{i,cv}^{n+1} &= \rho_{cv}^{n+1} \frac{u_{i,cv}^{RBM,n+1} - u_{i,cv}^{*n+1}}{\Delta t} \\ u_{i,cv}^{n+1} &= u_{i,cv}^{*n+1} + \frac{f_{i,cv}^{n+1} \Delta t}{\rho_{cv}^{n+1}} \end{aligned}$$

Note that the interpolations from material points to the cv centers provide a non-zero rigidity constraint force only in the particle domain.

This completes the advancement of the particle and velocity fields by one time-step. Extending the algorithm to multiple particles is straightforward. For multiple particles, the inter-particle collision force must be modeled to prevent the particles from penetrating each other. In case of multi-particle simulations, the accuracy of inter-particle interactions is determined by the collision model. Implementation and model details are given in detail by Glowinski *et al.* [12] and are not repeated here.

4. Results

4.1. Flow over a Fixed Sphere. Flow over a fixed sphere in a uniform stream is calculated to investigate the accuracy of the numerical scheme to predict the drag coefficient and wake effects at different Reynolds numbers. A sphere of diameter $D_p = 0.8$ units is placed at $(2, 0, 0)$ in a square domain of range $(0, -4, -4)$ to $(8, 4, 4)$ units. Uniform cubic grids (128^3) are used over the entire region. This gives around 12 grid points within the particle domain. The material volume resolution is set based on the ratio $\frac{\Delta}{\Delta_M} = 6$. Note that, in this study, the spherical particle is represented by cubic material volumes. Uniform flow of $U_\infty = 1$ units is imposed at the left boundary of the domain. A convective outflow boundary condition is imposed at the exit. Slip condition ($\frac{\partial u}{\partial N} = 0$; where N represents normal to the boundary), is imposed on the boundaries in the vertical and spanwise directions. The fluid viscosity is varied to simulate flow over a sphere at different Reynolds numbers. Since the sphere is fixed, the material volumes are assigned a velocity of $\mathbf{U}_P = 0$, $\Omega_P = 0$ and setting $\mathbf{U}_M^{RBM,n+1} = 0$ in evaluating the rigidity constraint of the numerical algorithm.

Figure 2 shows the instantaneous streamlines over the fixed sphere at different Reynolds numbers. The flow remains symmetric for low Reynolds numbers ($Re_p = 20, 40$, and 100). At $Re_p = 100$, the reverse flow patterns are clearly visible. At large Reynolds number $Re_p > 300$, the flow starts to become asymmetric, shedding unsteady vortices. Table 1 compares the drag coefficients on a sphere at different Reynolds numbers with those obtained from experimental correlations [32].

TABLE 1. Comparison of drag coefficients over a fixed sphere at different Reynolds numbers.

Re_p	C_D , Present	C_D , Experiment	Error (%)
10	4.25	4.2	1.19
20	2.665	2.61	2.1
40	1.771	1.735	2.07
100	1.118	1.087	2.86
600	0.58	0.523	9.43

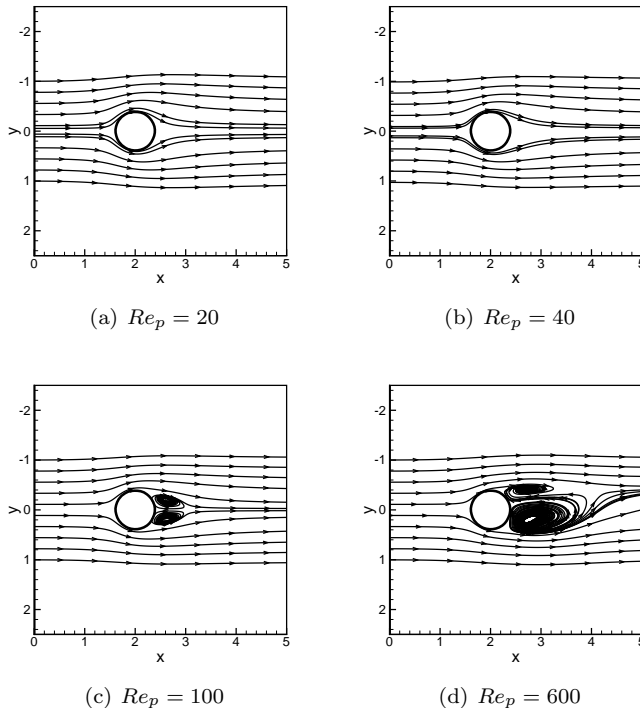


FIGURE 2. Instantaneous streamlines for flow over a fixed sphere at different Reynolds numbers.

The error in drag coefficient for low Reynolds numbers is less than 3%. The drag coefficient is consistently over-predicted. This may be attributed to the fact that the represented particle boundary is not perfectly spherical due to the cubical material volumes used. In addition, the boundary is smeared by the interpolation functions between the background grid and the material volumes. This has an indirect effect of making the sphere slightly larger than its actual diameter. Note that this error in spherical boundary representation can be reduced by increasing the number of material volumes (higher Δ/Δ_M ratio) or using material volumes conforming with the boundary of the sphere [31]. For large Reynolds numbers, ($Re_p = 600$) the background grid resolution of ($\Delta \approx D_p/12$) is not sufficient and affects the predicted drag coefficient. However, the algorithm is able to capture the asymmetric wake and unsteady vortex shedding as shown in Fig. 2. Accurate prediction of drag force can be obtained by further grid refinements. In most particle-laden turbulent flows, the particle Reynolds number is much lower (except for flows with high density ratios between the fluid and particle, e.g. air-particle) and a grid resolution of 10–12 points may be sufficient to capture the fluid-particle interactions.

4.2. Freely Falling Sphere. Freely falling solid sphere of density 3 kg/m^3 and diameter 0.625 m falling under gravity in a rectangular channel of cross-section $2 \text{ m} \times 2 \text{ m}$ and height 8 m is simulated. The fluid viscosity is 0.05 kg/m.s and the density is 2 kg/m^3 . Simulations were carried out for increasing grid refinement. The test case is same as that used by Sharma & Patankar [1] and validates our

numerical implementation in a colocated finite-volume scheme. Figure 3a shows the time evolution of the fluid velocity magnitude together with the location of the sphere. As seen from the velocity magnitudes, the adjacent walls do affect the overall drag on the particle. The blocking ratio defined as the ratio of the particle diameter to the channel cross-sectional length is 0.3125. The terminal velocity of the sphere considering the wall effects can be estimated using the correlations proposed in the literature [29, 28]. Accordingly, for the present case the terminal velocity is 1.2722 m/s.

Figure 3b shows the particle terminal velocity with grid refinement. Two different studies are considered: (a) keeping the Courant-Friedrichs-Lewis (CFL = 0.1) number fixed and (b) keeping the time step fixed ($\Delta t = 2.5 \times 10^{-3}$) with grid refinement. Five different grid resolutions ($\Delta = 1/25, 1/30, 1/40, 1/50, 1/60$) with cubical elements are used. The resolution of each material volume is fixed such that $\Delta/\Delta_M = 2$. The terminal velocity obtained with fixed CFL number is 1.288 whereas that with fixed time step is approximately 1.295. With fixed time-steps under grid refinement, the CFL number increases as the particle approaches its terminal velocity. Increased CFL numbers may lead to decreased accuracy over longer periods of time. However, with small CFL numbers, the numerical algorithm is able to predict the particle terminal velocity with good accuracy.

Figure 3c shows the time evolution of the particle velocity for CFL = 0.1 and grid resolution of $\Delta = 1/60$. The particle velocity is normalized by its terminal velocity and the time is normalized by the time it takes to reach 95% of the terminal velocity (t_{95}). This time evolution of the particle velocity is in qualitative agreement with the temporal behavior of sedimenting particle as observed by Mordant and Pinton [30]. The experiments were carried out at small blockage ratio (thus negligible wall effects) and thus quantitative comparison is not performed.

4.3. Particle Laden Isotropic Turbulent Flow. The numerical scheme is used to simulate particle-laden homogeneous, isotropic turbulent flow in a periodic box of length π with grid resolution of 128^3 . A stationary isotropic turbulent flow is first developed using linear forcing in the fluid momentum equations proportional to the local velocity [33]. The turbulence parameters correspond to the Reynolds number of 54 based on the Taylor microscale. The turbulence intensity is $U' = 0.84$, the dissipation rate $\epsilon = 0.2$, the fluid density $\rho = 1$, and the kinematic viscosity $\nu = 0.013$. This gives the Kolmogorov length scale of $\eta = 0.056$, the Kolmogorov time scale is $\tau_K = 0.25$ the Taylor microscale $\lambda = 0.81$, the integral length scale of $L = 1.65$, the integral time scale $T = 1.98$, and $k_{max}\eta$ (the measure of resolution) is 2.28. The time-step used is $\Delta t = 1 \times 10^{-3}$.

Once a stationary state is obtained, the forcing function is turned off and 125 solid cubic particles are injected into the domain, with initial uniform distribution. The length of the particles is 0.2 providing around 8 grid points over the particle domain. The particles are arranged such that they have a separation distance of $\frac{\pi}{5}$ between their nearest neighbors. The material volume resolution is based on the ratio $\frac{\Delta}{\Delta_M} = 3$. The particle density is $\rho_p = 9$ and the particle relaxation time is $\tau_p = \frac{1}{18} \frac{\rho_p}{\rho} \frac{\sigma^2}{\nu} \approx 0.9$, where σ is the characteristic length of the particle, and ν is the fluid viscosity. For the present case, the size of the particle is larger than the Kolmogorov length scale. Accordingly, different time scales can be used to normalize the particle relaxation time and define the Stokes number. Based on the Kolmogorov time-scale, the Stokes number, $St = \tau_p/\tau_K = 3.6$. The particle Reynolds number ($Re_p = \rho d_p |\mathbf{u}_{rel}|/\mu$), where \mathbf{u}_{rel} is the relative velocity between

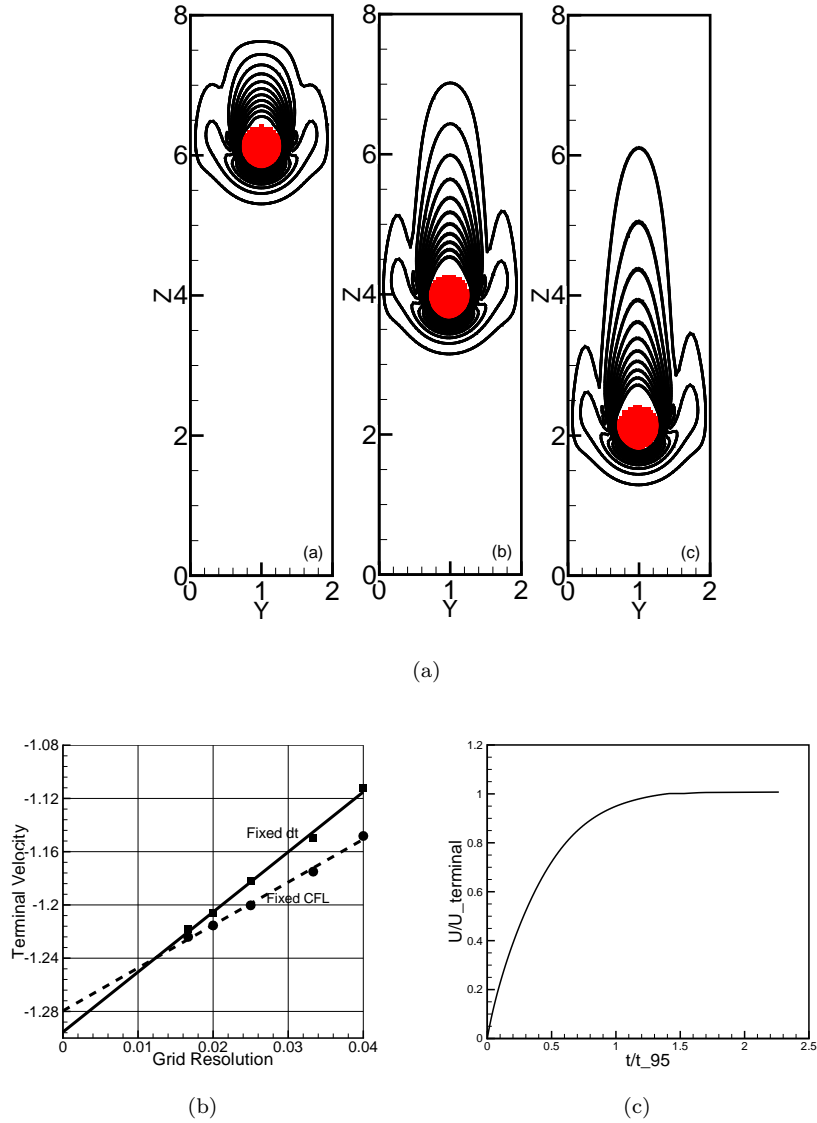


FIGURE 3. Simulation of a freely falling sphere under gravity: (a) time evolution of velocity magnitudes, (b) convergence study under grid refinement, and (c) time evolution of the particle velocity normalized by its terminal velocity. t_{95} corresponds to the particle response time or the time it takes for the particle to reach 95% of its terminal velocity.

the fluid and the particle, is on the order of 20–30 in these simulations. As was shown earlier for the flow over a fixed spherical particle, the resolution of 8–12 grid cells inside the particle domain is sufficient to resolve the fluid-particle interactions in this regime. As the turbulent flow decays, the particles first accelerate, reach a maximum velocity and then decelerate.

Figure 4 shows the time-evolution of the out-of-plane vorticity contours together with the location of the particles in the symmetry plane $z = 0$. Note that since a planar cut of instantaneous particle positions is shown, the particle boundary (as seen by red lines) may not appear as a square depending upon the instantaneous location of the particle centers. Accordingly, the shapes and sizes of the particles shown in the figures appear different. However, this is just the plotting artifact and in the simulations the particles retain their size. The particles cluster in low vorticity regions as they evolve from uniform distribution. Similar results have been reported for spherical particles in isotropic turbulent flow using the Lattice-Boltzmann approach [20]. The interactions between turbulence and particle motion is fully resolved and the numerical approach can be used for further investigations of particle-laden turbulent flows.

The simulation was performed on 64-processors (IBM machines at San Diego Supercomputing Center). It requires approximately 6 seconds per time-step for this simulation. The overhead of the computing time due to computation of the rigidity constraint, the motion of particles and inter-particle collisions is only 20% of the overall time. For the present case, since the particles are initially uniformly distributed, load balancing was not an issue. The grid was partitioned such that each processor has approximately the same number of grid points. However, for inhomogeneous distribution of large number of particles, such partitioning may result in parallel load imbalance and advanced domain decomposition concepts are necessary for improved computation. In addition, in the current approach, the material volumes are present over the entire region of the particle. This is done for simplicity in the implementation of the integrations over the particle domain and also characterization of the boundary of the particle. Use of material volumes in a small band around the particles (similar to the particle level set methods) to characterize the particle-boundaries, is possible and will reduce the number of material volumes required per particle. The integration over the particle domain then can be performed using the background grid and interpolation operations.

5. Discussion

A numerical formulation for fully resolved simulations of freely moving rigid particles in turbulent flows is developed based on a co-located grid, finite-volume method. In this fictitious domain based approach, the entire computational domain is first treated as a fluid of density corresponding to the fluid or particle densities in their respective regions. The incompressibility and rigidity constraints are applied to the fluid and particle regions, respectively, by using a fractional step algorithm. The approach extends the formulation developed by Patankar [21, 1] to obtain the rigid body motion without requiring any iterative procedures. Use of consistent interpolations between the particle material volumes and the background grid and parallel implementation of the algorithm facilitates accurate and efficient simulations of large number of particles. Implementation of this approach in finite-volume based, conservative numerical solvers is presented. The numerical approach is validated for flow over a fixed sphere at various Reynolds numbers and flow generated by a freely falling sphere under gravity to show good predictive capability. Finally, simulation of 125 cubical particles in a decaying isotropic turbulent flow is performed to study the feasibility of simulations of turbulent flows in the presence of freely moving, arbitrary-shaped rigid particles. The overhead due to presence of particles and computing their motion is small and the computational speed is governed by the pressure Poisson equation used to impose the incompressibility

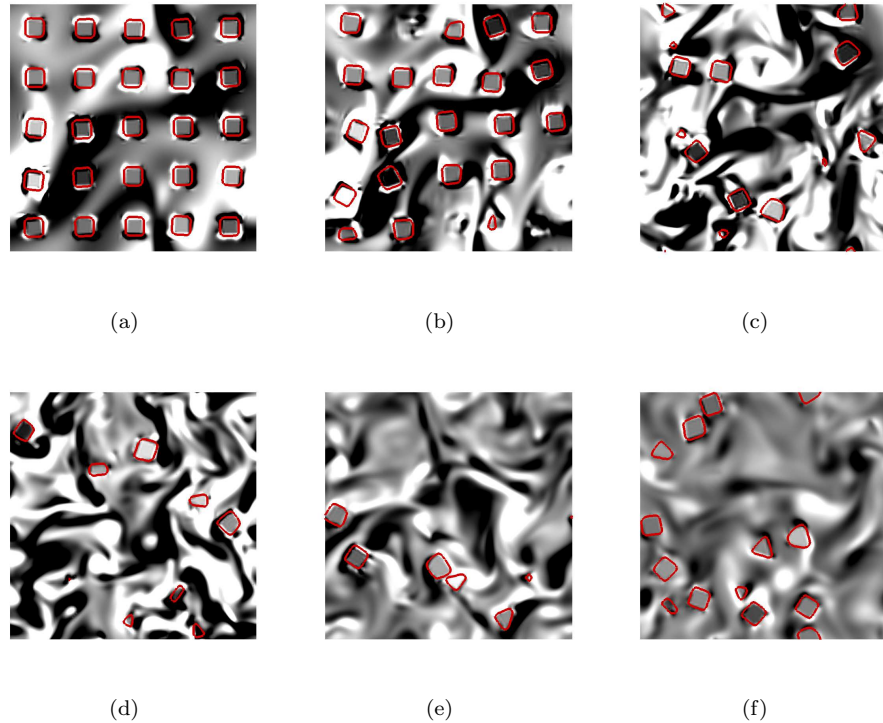


FIGURE 4. Temporal evolution of cubical particles in a decaying isotropic turbulent flow. The simulations are performed on a 128^3 grid and contains 125 cubical particles initially uniformly spaced. A planar cut in the $z = 0$ plane is shown, the contours indicate out-of-plane vorticity and red lines show particle shapes. Due to the planar cuts, the particle shapes *appear* different as the cubical particles move in and out of plane in this turbulent flow. The simulation was performed on 64 processors at San Diego Supercomputing Center.

constraint, making this approach attractive for large-scale simulations resolving the multiscale interactions between particles and turbulent flow.

Acknowledgments

The computing time at San Diego Supercomputing Center’s Datastar machine is highly appreciated. SVA acknowledges Dr. Ki-Han Kim of the Office of Naval Research for the summer support provided under the ONR grant number N000140610697, which resulted in successful completion of the numerical implementation of the algorithm. Past interactions with Prof. K. Mahesh of University of Minnesota and Dr. Frank Ham of Stanford University on co-located grid, fractional step methods are also appreciated.

References

- [1] SHARMA, N., & PATANKAR, N. A. 2005 A fast computation technique for the direct numerical simulation of rigid particulate flows., *J. Comp. Phy.*, **205** 439–457.

- [2] READE, W. C. & COLLINS, L. R. 2000 Effect of preferential concentration on turbulent collision rates. *Phys. Fluids* **12**, 2530–2540.
- [3] ROUSON, D. W. I. & EATON, J. K. 2001 On the preferential concentration of solid particles in turbulent channel flow. *J. Fluid Mech.* **348**, 149–169.
- [4] XU, J., DONG, S., MAXEY, M., & KARNIADAKIS, G., 2003 Direct numerical simulation of turbulent channel flow with bubbles, *Current Trends in Scientific Computing: ICM2002*, **329**, 347–354.
- [5] WANG, Q. & SQUIRES, K.D., 1996 Large-eddy simulation of particle-laden turbulent channel flow, *Phy. Fluids*, **8**, 1207–1223.
- [6] APTE, S. V., MAHESH, K., MOIN, P., & OEFELIN, J.C., 2003a, Large-eddy simulation of swirling particle-laden flows in a coaxial-jet combustor. *Int. J. Mult. Flow* **29**, 1311–1331.
- [7] SEGURA, J. C., EATON, J. K. & OEFELIN, J. C. 2004 Predictive capabilities of particle-laden LES. Rep. No. TSD–156, Dept. of Mech. Engr., Stanford University.
- [8] MOIN, P., & APTE S.V., 2006, Large eddy simulation of multiphase reacting flows in complex combustors, *AIAA J.*, **44**, 698–710 (special issue on ‘Combustion Modeling and LES: Development and Validation Needs for Gas Turbine Combustors’).
- [9] SOMMERFELD, M., ANDO, A., & QIU, H. H. 1992 Swirling, particle-laden flows through a pipe expansion *J. Fluids. Engr.* **114**, 648–656.
- [10] APTE, S.V., MAHESH, K., & LUNDGREN T., 2007 Accounting for Finite-Size Effects in Simulations of Two-Phase Flows *Int. J. Multiphase Flow* accepted for publication.
- [11] HU, H. H., PATANKAR, N.A., ZHU, M.Y., 2001, Direct numerical simulation of fluid-solid systems using the arbitrary Lagrangian-Eulerian technique, *J. Comp. Phys.*, **169**, 427–462.
- [12] GLOWINSKI, R. PAN, T.W., HESLA, T.I., JOSEPH, D.D., PERIAUX, J., 2001, A fictitious domain approach to the direct numerical simulation of incompressible viscous flow past moving rigid bodies: Application to particulate flow, *J. Comput. Phys.*, **169**, 363–426.
- [13] PATANKAR, N., SINGH, P., JOSEPH, D., GLOWINSKI, R., & PAN, T., 2000 A new formulation of the distributed Lagrange multiplier/fictitious domain method for particulate flows *Int. J. Multiphase Flow* **26**, 1509.
- [14] VEERAMANI, C., MINEV, P.D., & NANDAKUMAR, K., 2007, A fictitious domain formulation for flows with rigid particles: A non-Lagrange multiplier version, *J. Comp. Phys.*, **224**, 867–879.
- [15] LADD, A.J.C. & VERBERG, R., 2001 Lattice-Boltzmann simulations of particle-fluid suspensions, *J. STATIST. PHYS.*, **104**, 1191–1251.
- [16] ZHANG, Z. & PROSPERETTI, A., 2005 A second-order method for three-dimensional particle flow simulations, *J. Comput. Phys.*, **210**, 292–324.
- [17] FENG, Z-G, & MICHAELIDES, E.E., 2005, Proteus: a direct forcing method in the simulations of particulate flows, *J. Comp. Phys.*, **202**, 20–51.
- [18] TAIRA K., & COLONIUS, T., 2007, The immersed boundary method: A projection approach, *J. Comp. Phys.*, **225** (2), 2118–2137.
- [19] KAJISHIMA, T., TAKIGUCHI, S., & MIYAKE, Y., 1999, Modulation and subgrid scale modeling of gas-particle turbulent flow, in: D. Knight, L. Sakell (Eds.), *Recent Advances in DNS and LES*, Kluwer Academic Publishers, 235–244.
- [20] TEN CATE, A., DERKSEN, J.J., PORTELA L.M., & VAN DEN AKKER, H. E.A., 2004, Fully resolved simulations of colliding monodisperse spheres in forced isotropic turbulence, *J. Fluid Mech.*, **519**, 233–271.
- [21] PATANKAR, N. A. 2001 A formulation for fast computations of rigid particulate flows. *Annual Research Briefs Center Turbul. Res.*, 185–196.
- [22] PESKIN, C.S, 2002, The immersed boundary method, *Acta Numerica*, **11** 479–517.
- [23] MAHESH, K., CONSTANTINESCU, G., AND MOIN, P., 2004, A new time-accurate finite-volume fractional-step algorithm for prediction of turbulent flows on unstructured hybrid meshes, *J. Comp. Phys.*, **197**, 215–240.
- [24] KIM, D., & CHOI, H, 2000, A Second-Order Time-Accurate Finite Volume Method for Unsteady Incompressible Flow on Hybrid Unstructured Grids, *J. Comp. Phys.*, **162**, 411–428.
- [25] HAM, F., APTE, S.V., IACCARINO, G., WU, X., HERRMANN, M., CONSTANTINESCU, G., MAHESH, K., AND MOIN, P., 2003, Unstructured LES of reacting multiphase flows in realistic gas-turbine combustors, *Annual Research Briefs*, Center for Turbulence Research, Stanford University, 13–160, (<http://ctr.stanford.edu>).
- [26] MAHESH, K., CONSTANTINESCU, G., APTE, S.V., IACCARINO, G., HAM, F., AND MOIN, P., 2006 Large-eddy simulation of reacting turbulent flows in complex geometries, *ASME J. App. Mech.*, accepted for publication.

- [27] LAWRENCE AND LIVERMORE AND NATIONAL AND LABORATORY'S AND CASC AND TEAM 2006, Scalable linear solvers, HYPRE, http://www.llnl.gov/CASC/linear_solvers, *hypre2.0.0*.
- [28] BROWN, P.P. & LAWLER, D.F., 2003, Sphere drag and settling velocity revisited, *J. Environ. Engng.* **129**, 222–231.
- [29] FIDLERIS, V., & WHITMORE, R.L. 1961 Experimental determination of the wall effect for spheres falling axially in cylindrical vessels, *Br. J. Appl. Phys.* **12**, 490–494.
- [30] MORDANT, N. & PINTON, J.F., 2000, Velocity measurement of a settling sphere, *Eur. Phys. J. B* **18** 343–352.
- [31] YU, Z., SHAO, X., & WACHS, A., 2006, A fictitious domain method for particulate flows with heat transfer, *J. Comp. Phy.*, **217**, 424–452.
- [32] WHITE F. M., 1991, Viscous fluid flow, McGraw-Hill, New York.
- [33] LUNDGREN, T., 2003, Linearly forced isotropic turbulence, *Annual Research Briefs*, Center for Turbulence Research, Stanford University, 461–473, (<http://ctr.stanford.edu>).

Department of Mechanical Engineering, Oregon State University, Corvallis, OR 97331, USA
E-mail: sva@engr.orst.edu
URL: http://me.oregonstate.edu/people/faculty/therm_fluid/apte.html

Department of Mechanical Engineering, Northwestern University, Evanston, IL, USA
E-mail: n-patankar@northwestern.edu
URL: <http://www.mech.northwestern.edu/web/people/faculty/patankar.htm>